molecules

MDPI

Article

FeO_x-Modified Ultrafine Platinum Particles Supported on $MgFe_2O_4$ with High Catalytic Activity and Promising Stability toward Low-Temperature Oxidation of CO

Chanchan Wang [1,2,†], Fen Wang [1,2,*,†] and Jianjun Shi [1,2,*]

[1] School of Chemical and Blasting Engineering, Anhui University of Science and Technology, Huainan 232001, China; chanchanwang08@163.com
[2] Institute of Environment-Friendly Materials and Occupational Health of Anhui University of Science and Technology (Wuhu), Wuhu 241003, China
* Correspondence: fenwang@aust.edu.cn (F.W.); jjshi@aust.edu.cn (J.S.)
† These authors contributed equally to this work.

Abstract: Catalytic oxidation is widely recognized as a highly effective approach for eliminating highly toxic CO. The current challenge lies in designing catalysts that possess exceptional low-temperature activity and stability. In this work, we have prepared ultrafine platinum particles of ~1 nm diameter dispersed on a $MgFe_2O_4$ support and found that the addition of 3 wt.% FeO_x into the $3Pt/MgFe_2O_4$ significantly improves its activity and stability. At an ultra-low temperature of 30 °C, the CO can be totally converted to CO_2 over $3FeO_x$-$3Pt/MgFe_2O_4$. High and stable performances of CO-catalytic oxidation can be obtained at 60 °C on $3FeO_x$-$3Pt/MgFe_2O_4$ over 35 min on-stream at WHSV = 30,000 mL/(g·h). Based on a series of characterizations including BET, XRD, ICP, STEM, H_2-TPR, XPS, CO-DRIFT, O_2-TPD and CO-TPD, it was disclosed that the relatively high activity and stability of $3FeO_x$-$3Pt/MgFe_2O_4$ is due to the fact that the addition of FeO_x could facilitate the antioxidant capacity of Pt and oxygen mobility and increase the proportion of adsorbed oxygen species and the amounts of adsorbed CO. These results are helpful in designing Pt-based catalysts exhibiting higher activity and stability at low temperatures for the catalytic oxidation of CO.

Keywords: catalyst; ultrafine platinum particles; $MgFe_2O_4$; FeO_x modification; CO oxidation

check for updates

Citation: Wang, C.; Wang, F.; Shi, J. FeO_x-Modified Ultrafine Platinum Particles Supported on $MgFe_2O_4$ with High Catalytic Activity and Promising Stability toward Low-Temperature Oxidation of CO. *Molecules* **2024**, *29*, 1027. https://doi.org/10.3390/molecules29051027

Academic Editor: Ewa Kowalska

Received: 28 January 2024
Revised: 18 February 2024
Accepted: 22 February 2024
Published: 27 February 2024

Copyright: © 2024 by the authors. Licensee MDPI, Basel, Switzerland. This article is an open access article distributed under the terms and conditions of the Creative Commons Attribution (CC BY) license (https://creativecommons.org/licenses/by/4.0/).

1. Introduction

The incomplete combustion of carbon-containing compounds and some important industrial processes such as ironmaking and steelmaking, as well as vehicle exhaust, produce carbon monoxide (CO) widely [1,2]. CO is a highly toxic gas for humans, and exposure to ppm levels of CO in an enclosed environment can cause serious poisoning. In industry, the trace amounts of CO can poison the Fe-based ammonia-synthesis catalysts [3], Pt-based fuel cell [4] and hydrogenation [5] catalysts, and so on. Catalytic oxidation is recognized as a highly effective method for removing low concentrations of CO. The major challenge of CO catalytic oxidation is to design catalysts with outstanding performance at low temperatures.

The catalysts employed in CO oxidation mainly consisted of transition-metal oxides (such as CuO [6], MnO_2 [7] and Co_3O_4 [8]) and noble metal catalysts (like supported Au [9], Pt [10], Pd [11], and Rh [12]). The attractive activity and thermal stability of noble metal-based catalysts make them highly appealing for CO oxidation compared to transition-metal oxide catalysts. Among numerous reported noble metal-based catalysts, Pt-based catalysts have gained great interest in various catalytic oxidation reactions, including formaldehyde oxidation [13], CO oxidation [14], propane oxidation [15], and so on. It is well known that ultrafine platinum particles (<2 nm) can efficiently enhance the catalytic oxidation activity [16,17], probably owing to the increase in their surface area and the presence of

more edge and corner atoms. In addition, decreasing the size of platinum particles can significantly improve the Pt atom utilization efficiency, and therefore can save catalyst costs. The typical methods of preparing ultrafine metallic platinum particles are colloidal synthesis. However, the usage of organic capping agents during the colloidal synthesis process often blocks the catalytic active sites, thereby causing a decrease in catalytic activity. Therefore, using the capping agents-free synthesis method to prepare ultrafine metallic platinum particles is more advantageous. It was reported that FeO_x possesses an excellent ability to disperse Pt owing to the strong interaction of Pt–FeO_x species [18]. Considering the fact that the single metal oxide has a lower surface area and poorer thermal stability than spinel materials, the usages of iron-based spinel oxides such as $MgFe_2O_4$ to disperse Pt are very promising. Additionally, it has been reported that the incorporation of FeO_x as an additive can boost the activities of supported Pt catalysts in the oxidation of CO [19–21]. Thus, we expected that FeO_x modification further improves the activities of $MgFe_2O_4$-supported Pt catalysts.

In this paper, we developed FeO_x-modified $MgFe_2O_4$-supported Pt catalysts with ultra-small-sized Pt particles of ~1 nm. It was found that FeO_x modification significantly promotes the activity and stability of Pt/$MgFe_2O_4$ in the oxidation of CO reactions, and the CO conversion can reach 100.0% at the low temperature of 30 °C. The as-prepared catalyst structure was comprehensively characterized by using BET, ICP, XRD, STEM, H_2-TPR, XPS, CO-DRIFT, O_2-TPD, and CO-TPD. The results reveal that the interaction between FeO_x and Pt exists, and the transfer of electrons from Pt to FeO_x was determined. The incorporation of 3 wt.% FeO_x into the 3Pt/$MgFe_2O_4$ improved the antioxidant capacity of Pt, increased the ratio of adsorbed oxygen species and the adsorbed amount of CO and promoted oxygen mobility, which are regarded as the main reasons responsible for the higher performance for CO oxidation on 3FeO_x-3Pt/$MgFe_2O_4$.

2. Results

2.1. Catalyst Performance

Figure 1a displays the CO oxidation activities of 3Pt/$MgFe_2O_4$ and 3FeO_x-3Pt/$MgFe_2O_4$ at 30–70 °C at WHSV = 30,000 mL/(g·h). The conversion of CO over 3Pt/$MgFe_2O_4$ displayed an increase from 74.0% to 100.0% as the reaction temperature was elevated from 30 to 52 °C. However, the 100.0% conversion of CO was achieved within the range of 30–70 °C over 3FeO_x-3Pt/$MgFe_2O_4$. Figure 1b displays the catalytic stability of the 3Pt/$MgFe_2O_4$ and 3FeO_x-3Pt/$MgFe_2O_4$ catalysts in the CO oxidation reaction at 60 °C. It is obvious that the 3FeO_x-3Pt/$MgFe_2O_4$ catalyst displays a stable CO conversion of 100.0% during the total test time of 35 min, while the CO conversion over 3Pt/$MgFe_2O_4$ decreases from 100.0% to 84.2% in the last 29 min of the reaction. Based on the results provided above, it can be inferred that the incorporation of 3 wt.% FeO_x into 3Pt/$MgFe_2O_4$ is beneficial in enhancing the CO-oxidation performance.

2.2. Catalyst Characterization

The isotherms of nitrogen physical adsorption as well as the pore-size distribution curves for the fresh 3Pt/$MgFe_2O_4$ and 3FeO_x-3Pt/$MgFe_2O_4$ samples are presented in Figure 2. Both 3Pt/$MgFe_2O_4$ and 3FeO_x-3Pt/$MgFe_2O_4$ samples demonstrated type IV isotherms accompanied by hysteresis loops, which are indicative of their mesoporous structure (Figure 2a). The pore-size distributions plot also showed a mesoporous structure for both samples (Figure 2b). The corresponding properties of the 3Pt/$MgFe_2O_4$ and 3FeO_x-3Pt/$MgFe_2O_4$ are listed in Table 1. Based on the nitrogen-adsorption results, the specific surface areas for the 3Pt/$MgFe_2O_4$ and 3FeO_x-3Pt/$MgFe_2O_4$ samples are 93.8 and 77.9 m^2/g, respectively. Additionally, the average pore sizes were determined to be 11.3 and 11.5 nm, and the pore volumes were measured to be 0.29 and 0.25 cm^3/g for the 3Pt/$MgFe_2O_4$ and 3FeO_x-3Pt/$MgFe_2O_4$ samples, respectively. The Pt loadings, as determined by ICP-OES, are 3.1 and 2.9 wt.% for the fresh 3Pt/$MgFe_2O_4$ and 3FeO_x-3Pt/$MgFe_2O_4$, respectively.

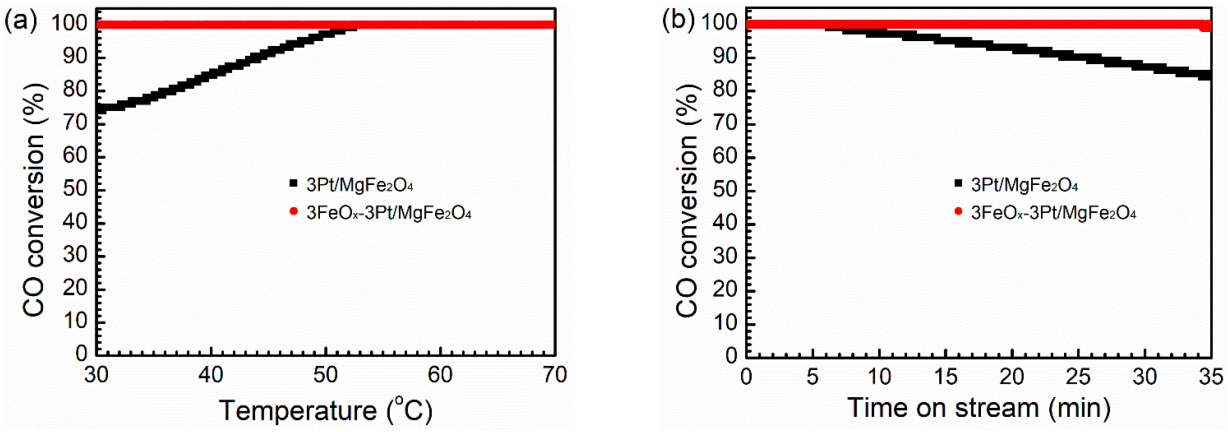

Figure 1. (**a**) CO catalytic-oxidation activities and (**b**) catalytic stability at 60 °C of $3Pt/MgFe_2O_4$ and $3FeO_x$-$3Pt/MgFe_2O_4$ at WHSV = 30,000 mL/(g·h).

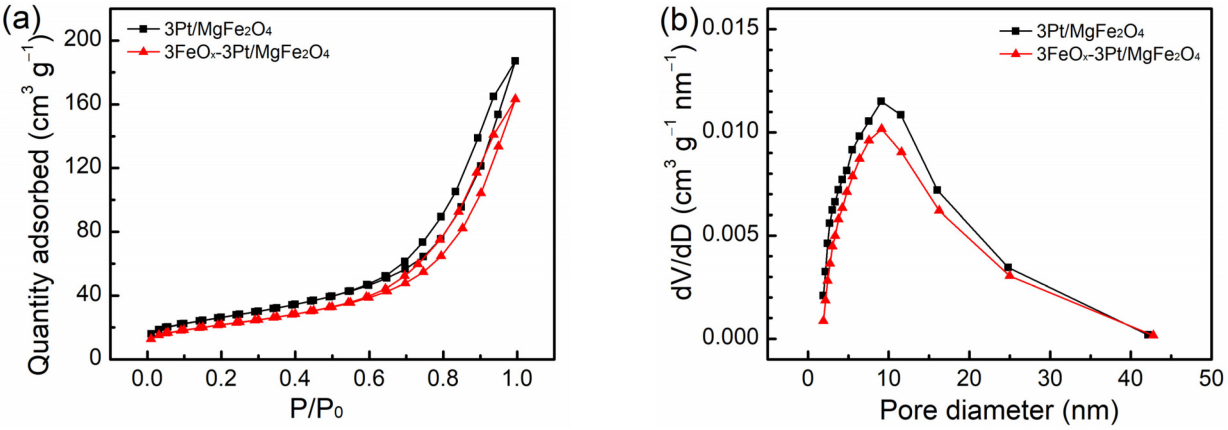

Figure 2. (**a**) Isotherms of nitrogen physical adsorption and (**b**) pore-size distribution plots for the fresh $3Pt/MgFe_2O_4$ and $3FeO_x$-$3Pt/MgFe_2O_4$.

Table 1. Properties of the $3Pt/MgFe_2O_4$ and $3FeO_x$-$3Pt/MgFe_2O_4$.

Samples	S_{BET} (m^2/g)	Pore Size [a] (nm)	Pore Volume (cm^3/g)	Pt Loading (wt.%)	d_{STEM} (nm)	(Pt^0) [b] %	(O_{ads}) [c] %	(Pt^0) [d] %	(O_{ads}) [e] %
$3Pt/MgFe_2O_4$	93.8	11.3	0.29	3.1	1.2	43.1	31.7	24.5	32.5
$3FeO_x$-$3Pt/MgFe_2O_4$	77.9	11.5	0.25	2.9	1.3	49.0	37.4	31.7	40.3

[a] Average pore size calculated from BJH desorption branch. [b] Proportion of Pt^0 in the fresh $3Pt/MgFe_2O_4$ and $3FeO_x$-$3Pt/MgFe_2O_4$ determined by the ratio of peak area according to $A_{Pt0}/(A_{Pt0} + A_{Pt2+} + A_{Pt4+})$. [c] Proportion of O_{ads} in the fresh $3Pt/MgFe_2O_4$ and $3FeO_x$-$3Pt/MgFe_2O_4$ determined by the ratio of peak area according to $A_{Oads}/(A_{Olatt} + A_{Oads})$. [d] Proportion of Pt^0 in the spent $3Pt/MgFe_2O_4$ and $3FeO_x$-$3Pt/MgFe_2O_4$ determined by the ratio of peak area according to $A_{Pt0}/(A_{Pt0} + A_{Pt2+} + A_{Pt4+})$. [e] Proportion of O_{ads} in the spent $3Pt/MgFe_2O_4$ and $3FeO_x$-$3Pt/MgFe_2O_4$ determined by the ratio of peak area according to $A_{Oads}/(A_{Olatt} + A_{Oads})$.

The XRD patterns for the fresh $3Pt/MgFe_2O_4$ and $3FeO_x$-$3Pt/MgFe_2O_4$ are presented in Figure 3. The characteristic diffraction peaks for $MgFe_2O_4$ (JCPDS 73-1720) can be observed in both $3Pt/MgFe_2O_4$ and $3FeO_x$-$3Pt/MgFe_2O_4$. In addition to $MgFe_2O_4$, no diffraction peak of Pt was observed on these two catalysts, suggesting that the sizes of Pt nanoparticles are smaller than that of the XRD detection limit (<3 nm). To further confirm this result, the STEM technique was employed. As shown in Figure 4a,d, both the fresh $3Pt/MgFe_2O_4$ and $3FeO_x$-$3Pt/MgFe_2O_4$ have high Pt-nanoparticle density with narrow size distributions. According to statistical data of over 200 Pt-nanoparticle sizes, the average sizes of Pt nanoparticles were determined to be 1.2 and 1.3 nm for $3Pt/MgFe_2O_4$ and $3FeO_x$-

3Pt/$MgFe_2O_4$, respectively. Pt nanoparticles in 3Pt/$MgFe_2O_4$ and 3FeO_x-3Pt/$MgFe_2O_4$ can be seen more clearly in Figure 4c,f.

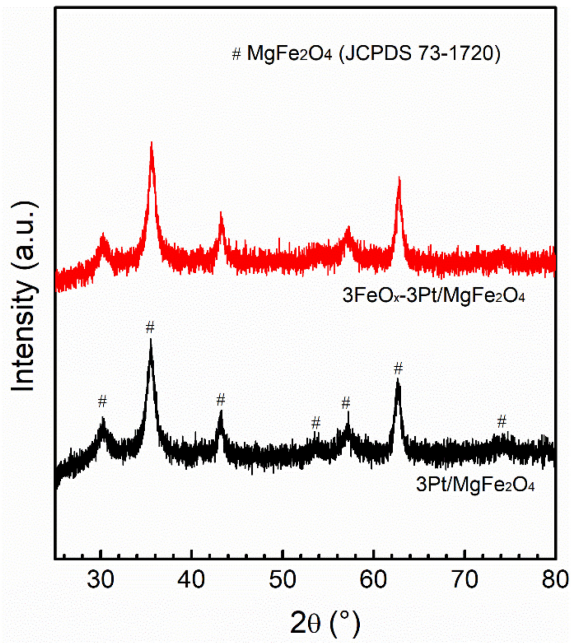

Figure 3. XRD patterns of the fresh 3Pt/$MgFe_2O_4$ and 3FeO_x-3Pt/$MgFe_2O_4$.

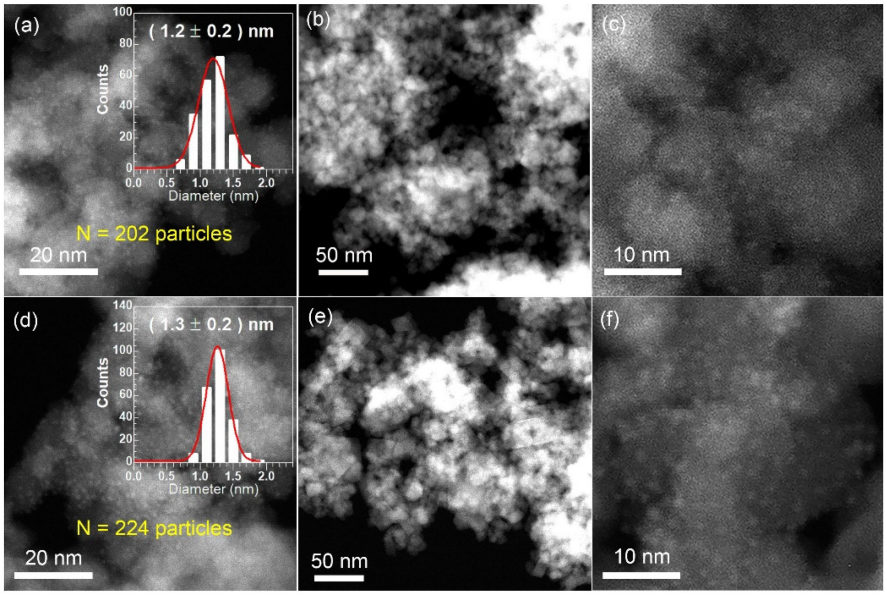

Figure 4. STEM images and the size histogram of Pt-particle distribution for the fresh (**a**–**c**) 3Pt/$MgFe_2O_4$ and (**d**–**f**) 3FeO_x-3Pt/$MgFe_2O_4$.

We conducted H_2-TPR experiments to explore in detail the reducibility of 3Pt/$MgFe_2O_4$ and 3FeO_x-3Pt/$MgFe_2O_4$ as well as $MgFe_2O_4$ support, and the obtained outcomes are illustrated in Figure 5. For $MgFe_2O_4$ support, the reduction peak above 250 °C belongs to the reduction of iron species because of the nonreducible of Mg^{2+}. For 3Pt/$MgFe_2O_4$ and 3FeO_x-3Pt/$MgFe_2O_4$, a distinct reduction peak was found at 90–150 °C in addition to a reduction peak above 250 °C, which belongs to the PtO_x reduction [22,23]. As shown in insert figure, the PtO_x reduction peak for 3Pt/$MgFe_2O_4$ and 3FeO_x-3Pt/$MgFe_2O_4$ is centered at 107 and 112 °C, respectively. The introduction of FeO_x to 3Pt/$MgFe_2O_4$ raises

the reduction temperature of PtO_x species obviously. It suggests that the interaction that exists between FeO_x and PtO_x and FeO_x is expected to modify the electron properties of metallic Pt nanoparticles.

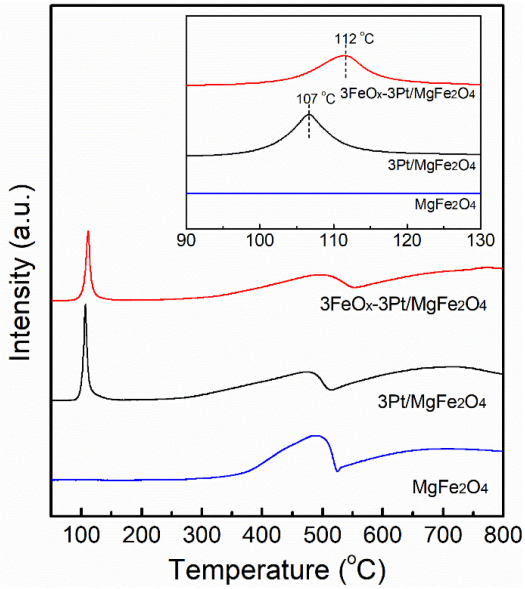

Figure 5. H_2-TPR diagrams of the calcined $3Pt/MgFe_2O_4$ and $3FeO_x$-$3Pt/MgFe_2O_4$ as well as $MgFe_2O_4$ support.

The valence states of platinum and the type of surface oxygen species in $3Pt/MgFe_2O_4$ and $3FeO_x$-$3Pt/MgFe_2O_4$ were explored using XPS. The XPS spectra for the Pt 4f orbitals of the fresh $3Pt/MgFe_2O_4$ and $3FeO_x$-$3Pt/MgFe_2O_4$ are presented in Figure 6a. These spectra can be fitted well with six peaks. The Pt 4f spectra of the fresh $3Pt/MgFe_2O_4$ exhibit two fitted peaks observed at binding energy values of 71.4 and 74.7 eV, which can be ascribed to Pt $4f_{7/2}$ and Pt $4f_{5/2}$ orbitals for Pt^0, respectively. Two fitted peaks observed at binding energy values of 72.3 and 75.5 eV can be associated with Pt $4f_{7/2}$ and Pt $4f_{5/2}$ orbitals for Pt^{2+}, respectively. The presence of two additional peaks observed at 74.1 and 77.7 eV can be assigned to Pt $4f_{7/2}$ and Pt $4f_{5/2}$ orbitals of the Pt^{4+} state, respectively [24–27]. Similar Pt species were observed in the fresh $3FeO_x$-$3Pt/MgFe_2O_4$ while their binding energy shifted to higher values by ~0.2 eV. This suggests that there is an interaction between Pt and FeO_x where the electrons are transferred from Pt to FeO_x. The existence of Pt^{2+} and Pt^{4+} in the fresh $3Pt/MgFe_2O_4$ and $3FeO_x$-$3Pt/MgFe_2O_4$ samples could be induced by the oxidation process with air at room temperature. According to the calculation of the proportion of the Pt^0 peak areas to the sum of the Pt^0, Pt^{2+} and Pt^{4+} peak areas, the relative amounts of Pt^0 in the fresh $3Pt/MgFe_2O_4$ and $3FeO_x$-$3Pt/MgFe_2O_4$ are 43.1% and 49.0%, respectively (Table 1). These findings indicate that FeO_x reduced the degree of reoxidation for the reduced-state Pt, which indirectly reflects the Pt–FeO_x interaction in the $3FeO_x$-$3Pt/MgFe_2O_4$ sample. Figure 6b presents the XPS spectra for the O 1s orbitals of the fresh $3Pt/MgFe_2O_4$ and $3FeO_x$-$3Pt/MgFe_2O_4$ samples. The spectra could be fitted well, with three peaks which are located at binding energy values of 529.6, 530.7 and 531.8 eV, respectively. The peak centered at the low binding energy of 529.6 eV corresponds to the lattice oxygen (O_{latt}), where the peaks centered at the high binding energies of 530.7 and 531.8 eV correspond to adsorbed oxygen (O_{ads}) species [28–30]. According to the proportion of the O_{ads} peak areas to the sum of the O_{latt} and O_{ads} peak areas, the respective proportions of O_{ads} in the fresh $3Pt/MgFe_2O_4$ and $3FeO_x$-$3Pt/MgFe_2O_4$ are 31.7% and 37.4%, respectively. This indicates that the $3FeO_x$-$3Pt/MgFe_2O_4$ possesses a higher percentage of adsorbed oxygen species, indicating the higher capacity to adsorb and activate molecular oxygen, and therefore leading to enhanced catalyst performance [21,31,32]. Figure 6c,d present the Pt 4f and O 1s XPS results for the spent $3Pt/MgFe_2O_4$ and $3FeO_x$-$3Pt/MgFe_2O_4$ catalysts.

In the spent $3Pt/MgFe_2O_4$ and $3FeO_x$-$3Pt/MgFe_2O_4$, the binding energies of Pt 4f and O 1s remained unchanged. The relative amounts of Pt^0 for the spent $3Pt/MgFe_2O_4$ and $3FeO_x$-$3Pt/MgFe_2O_4$ are 24.5% and 31.7%, respectively. The higher percentage of Pt^0 in the spent $3FeO_x$-$3Pt/MgFe_2O_4$ suggests that FeO_x can improve the antioxidant performance of $Pt/MgFe_2O_4$ in the reaction atmosphere, which always leads to a high CO oxidation performance [25]. The relative amounts of O_{ads} for the spent $3Pt/MgFe_2O_4$ and $3FeO_x$-$3Pt/MgFe_2O_4$ are 32.5% and 40.3%, respectively. Compared to the fresh $3Pt/MgFe_2O_4$ and $3FeO_x$-$3Pt/MgFe_2O_4$, the spent $3Pt/MgFe_2O_4$ and $3FeO_x$-$3Pt/MgFe_2O_4$ exhibits a higher content of adsorbed oxygen species. This indicates that the gaseous molecular oxygen could adsorb on the surface of the catalysts [33].

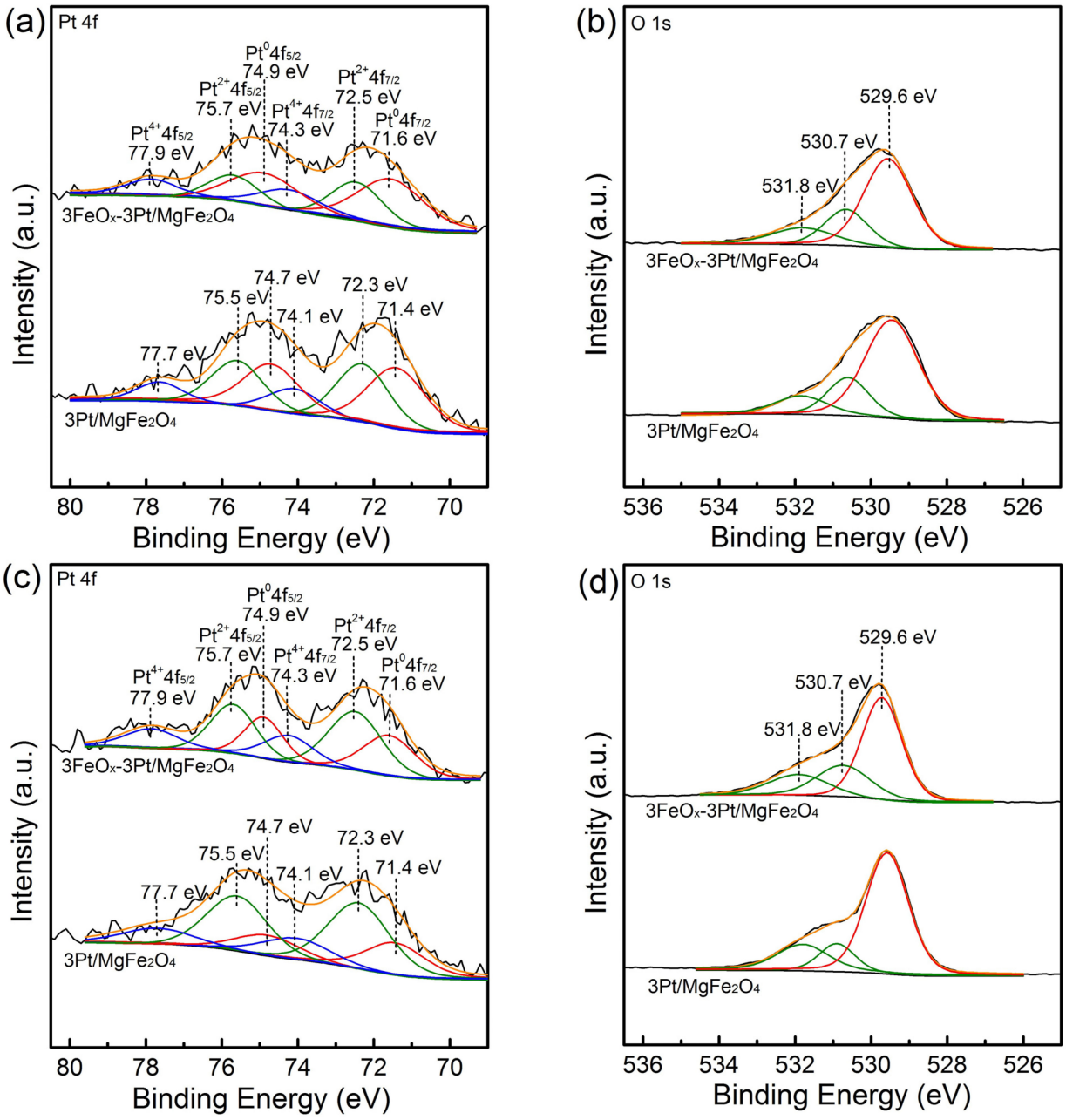

Figure 6. (**a**,**c**) Pt 4f and (**b**,**d**) O 1s XPS spectra for the (**a**,**b**) fresh and (**c**,**d**) spent $3Pt/MgFe_2O_4$ and $3FeO_x$-$3Pt/MgFe_2O_4$.

Figure 7 shows CO-DRIFT spectra of fresh $3Pt/MgFe_2O_4$ and $3FeO_x$-$3Pt/MgFe_2O_4$. Both $3Pt/MgFe_2O_4$ and $3FeO_x$-$3Pt/MgFe_2O_4$ show bands at 2173, 2060 and 1772 cm^{-1},

respectively. The band observed at 2173 cm^{-1} usually belongs to gaseous CO. The observed bands at 2060 and 1772 cm^{-1} are assigned to the linear and bridged CO adsorption on the surface of Pt^0 [33–37], respectively. The findings suggest that the Pt species are primarily present in the form of a Pt^0 metallic state in the pre-reduced catalysts. It is obvious that the CO bands' intensities at 2060 and 1772 cm^{-1} on the $3FeO_x$-$3Pt/MgFe_2O_4$ catalyst are much higher than those on the $3Pt/MgFe_2O_4$, indicating that the $3FeO_x$-$3Pt/MgFe_2O_4$ has a greater amount of adsorbed CO. $3FeO_x$-$3Pt/MgFe_2O_4$ with a high CO adsorption ability at 30 °C might result in an excellent CO-oxidation activity at low temperatures.

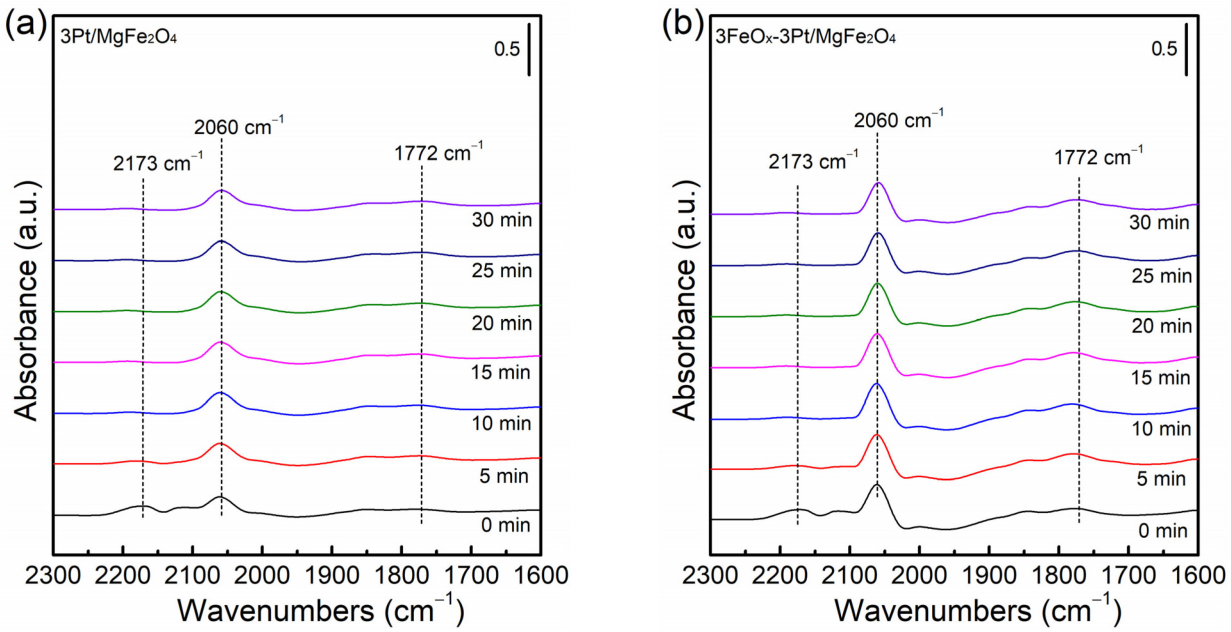

Figure 7. CO-DRIFT spectra of fresh (**a**) $3Pt/MgFe_2O_4$ and (**b**) $3FeO_x$-$3Pt/MgFe_2O_4$.

Figure 8a shows the O_2-TPD profiles of fresh $3Pt/MgFe_2O_4$ and $3FeO_x$-$3Pt/MgFe_2O_4$. The O_2-TPD profiles of $3Pt/MgFe_2O_4$ show oxygen desorption peaks at 154, 259, 555 and 776 °C, respectively. These desorption peaks shifted to lower temperatures of 136, 258, 546, and 748 °C for $3FeO_x$-$3Pt/MgFe_2O_4$, respectively. The lower oxygen desorption temperature in $3FeO_x$-$3Pt/MgFe_2O_4$ confirmed that $3FeO_x$-$3Pt/MgFe_2O_4$ has a higher oxygen mobility, which is advantageous to catalytic-CO oxidation. Figure 8b presents the CO-TPD profiles of fresh $3Pt/MgFe_2O_4$ and $3FeO_x$-$3Pt/MgFe_2O_4$. Both $3Pt/MgFe_2O_4$ and $3FeO_x$-$3Pt/MgFe_2O_4$ exhibited small desorption peaks of CO and large desorption peaks of CO_2. The formation of CO_2 may be related to the surface reaction of the adsorbed CO species with oxygen species. It has been observed that CO_2 formation in $3Pt/MgFe_2O_4$ begins at 125 °C, while for $3FeO_x$-$3Pt/MgFe_2O_4$, CO_2 formation occurs at 50 °C or even lower temperatures. The lower temperature at which CO_2 begins to form demonstrates that the oxygen species could be easily released and could participate in CO oxidation. Therefore, CO is much easier to be oxidized over $3FeO_x$-$3Pt/MgFe_2O_4$.

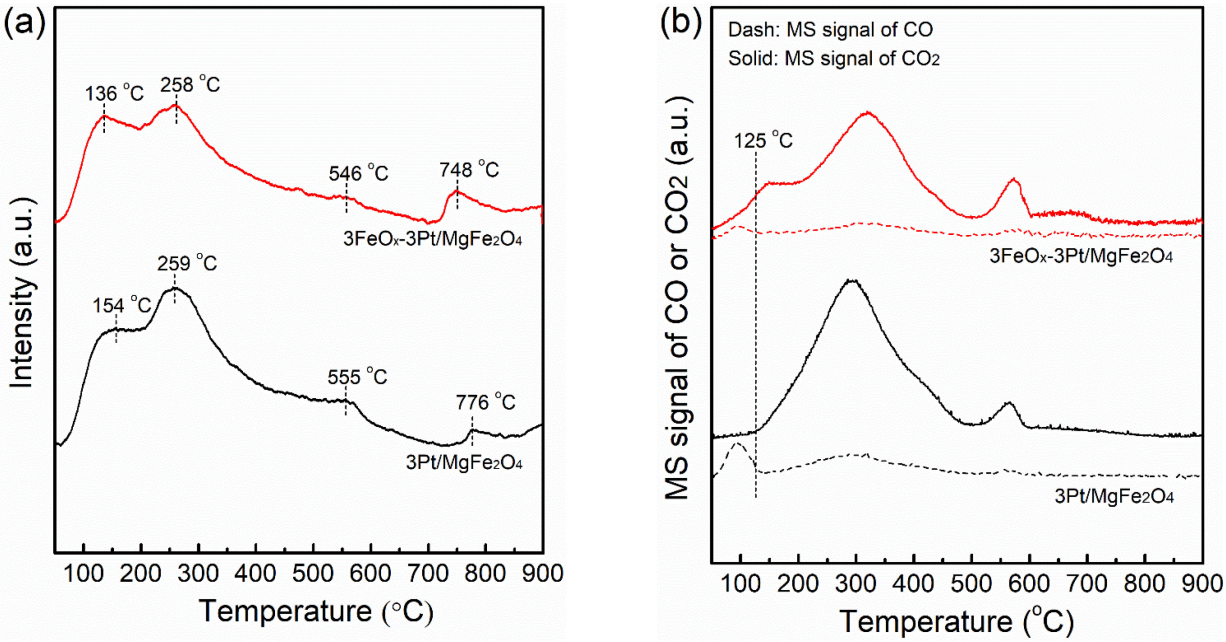

Figure 8. (**a**) O_2-TPD and (**b**) CO-TPD profiles of the fresh $3Pt/MgFe_2O_4$ and $3FeO_x$-$3Pt/MgFe_2O_4$.

3. Discussion

The introduction of FeO_x (3 wt.%) into $3Pt/MgFe_2O_4$ can greatly enhance its low-temperature catalytic activity and stability in CO oxidation. CO can be fully oxidized to CO_2 at temperatures as low as 30 °C over $3FeO_x$-$3Pt/MgFe_2O_4$ at WHSV = 30,000 mL/(g·h) (Figure 1a). At 30 °C, the CO-turnover rate on $3FeO_x$-$3Pt/MgFe_2O_4$ is calculated to be 0.024 mol/(mol_{Pt}-s), which is higher than the C-turnover rates reported in the literature (0.002 mol/(mol_{Pt}-s)) calculated at 50 °C on Pt/TiO_2 with high Pt oxidation state and a Pt size of less than 1 nm [38]. In addition, according to the literature reports, the CO-turnover rates at 30 °C on Pt/Nb_2O_5 modified with FeO_x with a Pt size of 3.5 nm is calculated to be 0.012 mol/(mol_{Pt}-s) [39], which is also lower than the CO-turnover rates on $3FeO_x$-$3Pt/MgFe_2O_4$. These results indicate that the FeO_x-modified ultrafine Pt nanoparticles (~1 nm) prepared in our article exhibit excellent low-temperature activity for the oxidation of CO. In addition, during the 35 min duration test for stability at 60 °C, the $3FeO_x$-$3Pt/MgFe_2O_4$ exhibited a high and constant CO conversion of 100.0% (Figure 1b). The nitrogen physical adsorption results indicated that the FeO_x modification might slightly decrease the surface area of $3Pt/MgFe_2O_4$ (Table 1). According to the XRD and STEM results (Figures 3 and 4, Table 1), the ultrafine Pt particles (~1 nm) are highly dispersed on the $MgFe_2O_4$ support for $3Pt/MgFe_2O_4$ and $3FeO_x$-$3Pt/MgFe_2O_4$, and FeO_x modification has little/no effect on the size of Pt. Based on the H_2-TPR- and XPS-characterization results (Figures 5 and 6), there is an interaction between FeO_x and Pt with an electron transfer from Pt to FeO_x. Moreover, the addition of FeO_x increased the ratio of the adsorbed oxygen species and decreased the oxidizing extent of the metallic Pt. The latter resulted in an increase in Pt^0 percentage in an oxidizing atmosphere. As we know, the Pt catalyst is present in an oxidizing atmosphere during a CO-oxidation reaction. The reduced Pt can be oxidized in this reaction mixture. It is generally believed that metallic Pt is more active in CO-oxidation reactions than in that of oxidized Pt [40,41]. The CO-DRIFT results demonstrated that the FeO_x modification increased the amount of CO adsorption on $3Pt/MgFe_2O_4$ (Figure 7). The results of O_2-TPD and CO-TPD showed that FeO_x promoted the oxygen mobility of $3Pt/MgFe_2O_4$ and CO_2 formation at low temperatures (Figure 8a,b). The high oxygen mobility in $3FeO_x$-$3Pt/MgFe_2O_4$ makes CO more easily oxidized, resulting in an outstanding catalytic performance for CO oxidation. The above results indicated that the incorporation of FeO_x into $Pt/MgFe_2O_4$ has successfully modified the electronic properties of Pt nanoparticles, while having almost no effect on the geometric structure of Pt

nanoparticles. The relatively strong antioxidant capacity, the high proportion of adsorbed oxygen species, and a high amount of adsorbed CO as well as the good oxygen mobility of $3FeO_x$-$3Pt/MgFe_2O_4$ contributed to its high low-temperature activity and improved stability for CO oxidation.

4. Materials and Methods

4.1. Catalyst Preparation

A solid-phase method was employed to synthesize the $MgFe_2O_4$ support. In brief, 0.015 M of $MgSO_4$ (Zesheng, Anqing, China), 0.03 M of $Fe(NO_3)_3 \cdot 9H_2O$ (Guoyao, Shanghai, China), 0.12 M of NaOH (Guoyao, Shanghai, China) and 0.15 M of NaCl (Annaiji, Shanghai, China) were simultaneously poured into a mortar and grinded evenly for 40 min. The obtained mixture was subjected to calcination at 700 °C for 1 h with a ramp rate of 2 °C/min. Subsequently, it was washed with deionized water and dried at 120 °C for 12 h.

The $Pt/MgFe_2O_4$ with Pt loading of 3 wt.% was synthesized through the incipient wetness impregnation of $MgFe_2O_4$ support with $H_2PtCl_6 \cdot 6H_2O$ (Damas-beta, Shanghai, China) dissolved in a certain amount of deionized water. After impregnation, the sample was subjected to drying at 60 °C under ambient air for 12 h and calcination at 500 °C in air for 5 h. After undergoing a repeated washing process with deionized water, the obtained solid was subjected to drying at 120 °C for 12 h and then reduction at 150 °C for 30 min in 5% H_2/N_2. Catalysts thus prepared were denoted as fresh $3Pt/MgFe_2O_4$.

FeO_x-modified $Pt/MgFe_2O_4$ with Fe loading of 3 wt.% (excluding the Fe content in $MgFe_2O_4$ support) was prepared by further incipient wetness impregnation of calcined $3Pt/MgFe_2O_4$ with the appropriate amount of $Fe(NO_3)_3 \cdot 9H_2O$ (Guoyao, Shanghai, China) dissolved in a certain amount of deionized water. After impregnation, the sample was treated in the same way as the $3Pt/MgFe_2O_4$, obtaining the fresh $3FeO_x$-$3Pt/MgFe_2O_4$ catalyst. The catalysts after the stability test of 60 °C were denoted as the spent $3Pt/MgFe_2O_4$ and $3FeO_x$-$3Pt/MgFe_2O_4$.

4.2. Catalyst Characterization

We conducted the surface-area testing of the as-prepared samples on a Micromeritics ASAP 2460 model adsorption instrument (Norcross, GA, USA). The Bruauer–Emmett–Teller (BET) method was employed with nitrogen as an adsorbate.

The content of Pt in the as-prepared samples was measured using inductively coupled plasma optical emission spectrometry (ICP-OES) with an Agilent 5110 instrument (Santa Clara, CA, USA).

We obtained X-ray diffraction (XRD) patterns of the as-prepared samples using a Rigaku SmartLab SE apparatus (Tokyo, Japan). The Cu Kα radiation with a wavelength of 0.15406 nm was utilized as the excitation source.

A JEOL JEM-2100F instrument (Tokyo, Japan) was employed to acquire the scanning transmission electron microscopy (STEM) images.

A Micromeritics AutoChem II 2920 instrument (Norcross, GA, USA) was utilized for performing the temperature-programmed reduction of H_2 (H_2-TPR). The sample (~0.1 g) was introduced into a quartz tube and maintained at 300 °C for 30 min under an Ar atmosphere. Subsequently, the sample was exposed to a 10% H_2/Ar and the temperature was gradually elevated to 800 °C using a ramp rate of 10 °C/min.

X-ray photoelectron spectroscopy (XPS) was determined by employing an Al Kα X-ray on a Thermo Fisher ESCALAB 250 Xi apparatus (Waltham, MA, USA). A reference of the C 1s peak at 284.6 eV was employed to correct all the obtained binding energies.

A Bruker Tensor 27 spectrometer (Ettlingen, Germany) was employed to record the in situ CO-diffuse reflectance infrared Fourier transform (CO-DRIFT) spectroscopy. The sample was subjected to reduction in a H_2 atmosphere at 150 °C for a duration of 30 min before CO adsorption. After cooling down to 30 °C under Ar, 20% CO/Ar of 30 mL/min was passed through the sample until the saturated adsorption of CO was reached. The 20% CO/Ar was subsequently switched to Ar and the data was collected.

The Micromeritics AutoChem II 2920 apparatus (Norcross, GA, USA) was utilized to conduct temperature-programmed desorption of O_2 (O_2-TPD). The sample (~0.1 g) was firstly subjected to reduction in a 10% H_2/Ar atmosphere at 150 °C for a duration of 30 min. After cooling down to 60 °C under Ar, 3% O_2/He was introduced for a duration of 1 h to achieve the saturated adsorption of O_2. Finally, the sample was subjected to a heating process up to 900 °C in the presence of an Ar atmosphere, and the data was recorded.

The Microtrac Belcat II apparatus (Osaka, Japan) was utilized to conduct temperature-programmed desorption (TPD) of CO. A 0.1 g sample was subjected to prereduction in a 10% H_2/Ar atmosphere at 150 °C for a duration of 30 min. After the temperature decreased to 50 °C in the presence of an Ar atmosphere, 10% CO/He was introduced for 1 h for the saturated adsorption of CO. Finally, the sample was subjected to heating up to 900 °C in Ar, and the mass signals corresponding to CO with m/z of 28 and CO_2 with m/z of 44 were recorded.

4.3. Catalytic Performance Tests

The oxidation of CO was conducted at atmospheric pressure in a U-shaped quartz fixed-bed reactor. Prior to the catalytic testing, all samples were exposed to 5% H_2/N_2 of 150 °C for a duration of 30 min for reduction. For each activity and stability test, a mixture consisting of 50 mg of catalysts and 1g of quartz sand was utilized. The reactant mixture consisted of 1% CO, 1% O_2 and 98% N_2. The total flow rate was 25 mL/min, which corresponded to a weighted hourly space velocity (WHSV) of 30,000 mL/(g·h). An FGA 10 model infrared gas analyzer was employed to monitor online the concentrations of reactants and products. We calculated the CO conversion as $(C_{CO,\ inlet} - C_{CO,\ outlet})/C_{CO,\ inlet} \times 100\%$, in which $C_{CO,\ inlet}$ and $C_{CO,\ outlet}$ represent the inlet and outlet CO concentrations of the reactor, respectively.

5. Conclusions

To summarize, we successfully synthesized a $3FeO_x$-$3Pt/MgFe_2O_4$ catalyst with ultrafine Pt particles that had an average size of ~1 nm. The incorporation of FeO_x into the $Pt/MgFe_2O_4$ catalyst significantly boosted the low-temperature catalytic activity and stability of the Pt catalyst for CO oxidation. CO conversion could reach 100.0% on $3FeO_x$-$3Pt/MgFe_2O_4$ at temperatures as low as 30 °C, and the elevated stability was obtained with a CO conversion of 100.0% at 60 °C for a 35 min run under a WHSV of 30,000 mL/(g·h). It was found that modifying $3Pt/MgFe_2O_4$ with FeO_x tunes the electronic properties while hardly changing the size of the Pt particles. Compared with $3Pt/MgFe_2O_4$, the remarkably increased catalytic performance of $3FeO_x$-$3Pt/MgFe_2O_4$ for CO oxidation might be attributed to its relatively strong antioxidant capacity, high ratio of adsorbed oxygen species, a greater amount of adsorbed CO, and an increased oxygen mobility. Overall, a deeper understanding of the crucial structure of catalysts needed for oxidizing CO in this work will contribute significantly to the advancement of a more high-performance Pt-based catalyst for the oxidation of CO.

Author Contributions: Conceptualization, C.W., F.W. and J.S.; methodology, C.W. and F.W.; validation, C.W.; investigation, C.W. and F.W.; data curation, C.W.; writing—original draft preparation, C.W. and F.W.; writing—review and editing, F.W. and J.S.; supervision, F.W. and J.S.; project administration, F.W. and J.S.; funding acquisition, F.W. All authors have read and agreed to the published version of the manuscript.

Funding: This research was supported by the Natural Science Research Project of Colleges and Universities in Anhui Province (2023AH051207), the National Natural Science Foundation of China (22308007), the Anhui Provincial Natural Science Foundation (2108085QB49) and the Research Foundation of the Institute of Environment-friendly Materials and Occupational Health of Anhui University of Science and Technology (Wuhu) (ALW2022YF05).

Institutional Review Board Statement: Not applicable.

Informed Consent Statement: Not applicable.

Data Availability Statement: Data are contained within the article.

Conflicts of Interest: The authors declare no conflicts of interest.

References

1. Wang, K.; Tian, H.; Hua, S.; Zhu, C.; Gao, J.; Xue, Y.; Hao, J.; Wang, Y.; Zhou, J. A comprehensive emission inventory of multiple air pollutants from iron and steel industry in China: Temporal trends and spatial variation characteristics. *Sci. Total Environ.* **2016**, *559*, 7–14. [CrossRef] [PubMed]
2. Liu, X.; Zou, Y.; Li, X.; Xu, T.; Cen, W.; Li, B.; Zhu, T. Ultralow doping of Mn species into Pt catalyst enhances the CO oxidation performance in the presence of H_2O and SO_2. *ACS Catal.* **2023**, *13*, 14580–14597. [CrossRef]
3. Waugh, K.C.; Butler, D.; Hayden, B.E.J.C.L. The mechanism of the poisoning of ammonia synthesis catalysts by oxygenates O_2, CO and H_2O: An in situ method for active surface determination. *Catal. Lett.* **1994**, *24*, 197–210. [CrossRef]
4. Liu, K.; Wang, A.; Zhang, T. Recent advances in preferential oxidation of CO reaction over platinum group metal catalysts. *ACS Catal.* **2012**, *2*, 1165–1178. [CrossRef]
5. Lin, L.; Yao, S.; Gao, R.; Liang, X.; Yu, Q.; Deng, Y.; Liu, J.; Peng, M.; Jiang, Z.; Li, S.; et al. A highly CO-tolerant atomically dispersed Pt catalyst for chemoselective hydrogenation. *Nat. Nanotechnol.* **2019**, *14*, 354–361. [CrossRef] [PubMed]
6. Fang, Y.; Chi, X.; Li, L.; Yang, J.; Liu, S.; Lu, X.; Xiao, W.; Wang, L.; Luo, Z.; Yang, W.; et al. Elucidating the nature of the Cu (I) active site in CuO/TiO_2 for excellent low-temperature CO oxidation. *ACS Appl. Mater. Interfaces* **2020**, *12*, 7091–7101. [CrossRef]
7. Liang, S.; Teng, F.; Bulgan, G.; Zong, R.; Zhu, Y. Effect of phase structure of MnO_2 nanorod catalyst on the activity for CO oxidation. *J. Phys. Chem. C* **2008**, *112*, 5307–5315. [CrossRef]
8. Zhou, M.; Cai, L.; Bajdich, M.; García-Melchor, M.; Li, H.; He, J.; Wilcox, J.; Wu, W.; Vojvodic, A.; Zheng, X. Enhancing catalytic CO oxidation over Co_3O_4 nanowires by substituting Co^{2+} with Cu^{2+}. *ACS Catal.* **2015**, *5*, 4485–4491. [CrossRef]
9. Kim, H.Y.; Lee, H.M.; Henkelman, G. CO oxidation mechanism on CeO_2-supported Au nanoparticles. *J. Am. Chem. Soc.* **2012**, *134*, 1560–1570. [CrossRef] [PubMed]
10. Allian, A.D.; Takanabe, K.; Fujdala, K.L.; Hao, X.; Truex, T.J.; Cai, J.; Buda, C.; Neurock, M.; Iglesia, E. Chemisorption of CO and mechanism of CO oxidation on supported platinum nanoclusters. *J. Am. Chem. Soc.* **2011**, *133*, 4498–4517. [CrossRef] [PubMed]
11. Duan, Z.; Henkelman, G. CO oxidation on the Pd (111) surface. *ACS Catal.* **2014**, *4*, 3435–3443. [CrossRef]
12. Guan, H.; Lin, J.; Qiao, B.; Yang, X.; Li, L.; Miao, S.; Liu, J.; Wang, A.; Wang, X.; Zhang, T. Catalytically active Rh sub-nanoclusters on TiO_2 for CO oxidation at cryogenic temperatures. *Angew. Chem. Int. Ed.* **2016**, *55*, 2820–2824. [CrossRef] [PubMed]
13. Chen, S.; Gueddida, S.; Badawi, M.; Lebègue, S.; Giraudon, J.-M.; Dhainaut, J.; Royer, S.; Lamonier, J.-F. Unravelling the critical role of silanol in Pt/SiO_2 for room temperature HCHO oxidation: An experimental and DFT study. *Appl. Catal. B Environ.* **2023**, *331*, 122672. [CrossRef]
14. Xu, L.; Pan, Y.; Li, H.; Xu, R.; Sun, Z. Highly active and water-resistant lanthanum-doped platinum-cobalt oxide catalysts for CO oxidation. *Appl. Catal. B Environ.* **2023**, *331*, 122678. [CrossRef]
15. Wang, X.-F.; Xu, L.-Y.; Wen, C.-H.; Li, D.-D.; Li, B.; Lu, J.-Q.; Yang, Q.-H.; Luo, M.-F.; Chen, J. WO_3 boosted water tolerance of Pt nanoparticle on SO_4^{2-}-ZrO_2 for propane oxidation. *Appl. Catal. B Environ.* **2023**, *338*, 123000. [CrossRef]
16. Lu, J.; Stair, P.C. Low-temperature ABC-type atomic layer deposition: Synthesis of highly uniform ultrafine supported metal nanoparticles. *Angew. Chem. Int. Ed.* **2010**, *49*, 2547–2551. [CrossRef] [PubMed]
17. Vajda, S.; Pellin, M.; Greeley, J.; Marshall, C.; Curtiss, L.; Ballentine, G.; Elam, J.; Catillon-Mucherie, S.; Redfern, P.; Mehmood, F.; et al. Subnanometre platinum clusters as highly active and selective catalysts for the oxidative dehydrogenation of propane. *Nat. Mater.* **2009**, *8*, 213–216. [CrossRef] [PubMed]
18. Qiao, B.; Wang, A.; Yang, X.; Allard, L.F.; Jiang, Z.; Cui, Y.; Liu, J.; Li, J.; Zhang, T. Single-atom catalysis of CO oxidation using Pt_1/FeO_x. *Nat. Chem.* **2011**, *3*, 634–641. [CrossRef]
19. Siani, A.; Alexeev, O.S.; Captain, B.; Lafaye, G.; Marécot, P.; Adams, R.D.; Amiridis, M.D. Synthesis of cluster-derived $PtFe/SiO_2$ catalysts for the oxidation of CO. *J. Catal.* **2008**, *255*, 162–179. [CrossRef]
20. Tomita, A.; Shimizu, K.-i.; Kato, K.; Tai, Y. Pt/Fe-containing alumina catalysts prepared and treated with water under moderate conditions exhibit low-temperature CO oxidation activity. *Catal. Commun.* **2012**, *17*, 194–199. [CrossRef]
21. Song, S.; Wu, Y.; Ge, S.; Wang, L.; Wang, Y.; Guo, Y.; Zhan, W.; Guo, Y. A facile way to improve Pt atom efficiency for CO oxidation at low temperature: Modification by transition metal oxides. *ACS Catal.* **2019**, *9*, 6177–6187. [CrossRef]
22. Tang, Z.; Liu, P.; Cao, H.; Bals, S.; Heeres, H.J.; Pescarmona, P.P. Pt/ZrO_2 prepared by atomic trapping: An efficient catalyst for the conversion of glycerol to lactic acid with concomitant transfer hydrogenation of cyclohexene. *ACS Catal.* **2019**, *9*, 9953–9963. [CrossRef]
23. Meher, S.K.; Cargnello, M.; Troiani, H.; Montini, T.; Rao, G.R.; Fornasiero, P. Alcohol induced ultra-fine dispersion of Pt on tuned morphologies of CeO_2 for CO oxidation. *Appl. Catal. B Environ.* **2013**, *130*, 121–131. [CrossRef]
24. Wang, F.; Ouyang, Y.; Yang, X. Promoting effect of Pt on the activity and stability of $Pd/MgFe_2O_4$ for catalytic combustion of methane. *J. Energy Inst.* **2023**, *110*, 101341. [CrossRef]
25. Liu, Y.-R.; Li, X.; Liao, W.-M.; Jia, A.-P.; Wang, Y.-J.; Luo, M.-F.; Lu, J.-Q. Highly active Pt/BN catalysts for propane combustion: The roles of support and reactant-induced evolution of active sites. *ACS Catal.* **2019**, *9*, 1472–1481. [CrossRef]

26. Li, J.; Guan, Q.; Wu, H.; Liu, W.; Lin, Y.; Sun, Z.; Ye, X.; Zheng, X.; Pan, H.; Zhu, J.; et al. Highly active and stable metal single-atom catalysts achieved by strong electronic metal–support interactions. *J. Am. Chem. Soc.* **2019**, *141*, 14515–14519. [CrossRef] [PubMed]
27. Zhao, P.-P.; Chen, J.; Yu, H.-B.; Cen, B.-H.; Wang, W.-Y.; Luo, M.-F.; Lu, J.-Q. Insights into propane combustion over MoO_3 promoted Pt/ZrO_2 catalysts: The generation of Pt-MoO_3 interface and its promotional role on catalytic activity. *J. Catal.* **2020**, *391*, 80–90. [CrossRef]
28. Zhang, X.; Liu, Y.; Deng, J.; Yu, X.; Han, Z.; Zhang, K.; Dai, H. Alloying of gold with palladium: An effective strategy to improve catalytic stability and chlorine-tolerance of the 3DOM CeO_2-supported catalysts in trichloroethylene combustion. *Appl. Catal. B Environ.* **2019**, *257*, 117879. [CrossRef]
29. Chen, Y.; Lin, J.; Chen, X.; Fan, S.; Zheng, Y. Engineering multicomponent metal-oxide units for efficient methane combustion over palladium-based catalysts. *Catal. Sci. Technol.* **2021**, *11*, 152–161. [CrossRef]
30. Xie, S.; Deng, J.; Zang, S.; Yang, H.; Guo, G.; Arandiyan, H.; Dai, H. Au–Pd/3DOM Co_3O_4: Highly active and stable nanocatalysts for toluene oxidation. *J. Catal.* **2015**, *322*, 38–48. [CrossRef]
31. He, J.; Chen, D.; Li, N.; Xu, Q.; Li, H.; He, J.; Lu, J. Pt–Pd bimetallic nanoparticles anchored on uniform mesoporous MnO_2 sphere as an advanced nanocatalyst for highly efficient toluene oxidation. *Green Energy Environ.* **2022**, *7*, 1349–1360. [CrossRef]
32. Wang, Y.; Arandiyan, H.; Tahini, H.A.; Scott, J.; Tan, X.; Dai, H.; Gale, J.D.; Rohl, A.L.; Smith, S.C.; Amal, R. The controlled disassembly of mesostructured perovskites as an avenue to fabricating high performance nanohybrid catalysts. *Nat. Commun.* **2017**, *8*, 15553. [CrossRef]
33. Zhu, M.-T.; Zhang, K.-F.; Du, W.-P.; Jia, A.-P.; Luo, M.-F.; Lu, J.-Q. Highly active and water tolerant Pt/MFe_2O_4 (M = Co and Ni) catalysts for low temperature CO oxidation. *Appl. Catal. A Gen.* **2021**, *619*, 118142. [CrossRef]
34. Peng, R.; Sun, X.; Li, S.; Chen, L.; Fu, M.; Wu, J.; Ye, D. Shape effect of Pt/CeO_2 catalysts on the catalytic oxidation of toluene. *Chem. Eng. J.* **2016**, *306*, 1234–1246. [CrossRef]
35. Kim, M.H.; Ebner, J.R.; Friedman, R.M.; Vannice, M.A. Dissociative N_2O adsorption on supported Pt. *J. Catal.* **2001**, *204*, 348–357. [CrossRef]
36. Meunier, F.C.; Cardenas, L.; Kaper, H.; Šmíd, B.; Vorokhta, M.; Grosjean, R.; Aubert, D.; Dembélé, K.; Lunkenbein, T. Synergy between metallic and oxidized Pt sites unravelled during room temperature CO oxidation on Pt/Ceria. *Angew. Chem. Int. Ed.* **2021**, *60*, 3799–3805. [CrossRef] [PubMed]
37. Zhao, P.; Wang, W.; Wang, X.; Liu, C.; Lu, J.; Luo, M.; Chen, J. The effects of MoO_3 impregnation order on the catalytic activity for propane combustion over Pt/ZrO_2 catalysts: The crucial roles of Pt–MoO_3 interfacial sites density. *New J. Chem.* **2021**, *45*, 14695–14702. [CrossRef]
38. Zhang, L.; Cheng, X.; Zhang, G.; Qiu, W.; He, H.; Chen, G. High active platinum clusters on titanium dioxide supports toward carbon monoxide oxidation. *Appl. Catal. B Environ.* **2020**, *266*, 118629. [CrossRef]
39. Li, B.; Wang, X.-F.; Wang, W.-Y.; Liu, C.-F.; He, L.-C.; Luo, M.-F.; Chen, J. Identifying the surface active sites of FeO_x-modified Pt/Nb_2O_5 catalysts in CO and propane oxidation. *Appl. Catal. A Gen.* **2023**, *649*, 118960. [CrossRef]
40. Jeong, H.; Shin, D.; Kim, B.-S.; Bae, J.; Shin, S.; Choe, C.; Han, J.W.; Lee, H. Controlling the oxidation state of Pt single atoms for maximizing catalytic activity. *Angew. Chem. Int. Ed.* **2020**, *59*, 20691–20696. [CrossRef]
41. Kim, G.J.; Kwon, D.W.; Hong, S.C. Effect of Pt particle size and valence state on the performance of Pt/TiO_2 catalysts for CO oxidation at room temperature. *J. Phys. Chem. C* **2016**, *120*, 17996–18004. [CrossRef]

Disclaimer/Publisher's Note: The statements, opinions and data contained in all publications are solely those of the individual author(s) and contributor(s) and not of MDPI and/or the editor(s). MDPI and/or the editor(s) disclaim responsibility for any injury to people or property resulting from any ideas, methods, instructions or products referred to in the content.